Journal of Alloys and Compounds 509 (2011) 2544–2551

Contents lists available at ScienceDirect

Journal of Alloys and Compounds

journal homepage: www.elsevier.com/locate/jallcom

Dependence of Eu^{3+} luminescence dynamics on the structure of the combustion synthesized $Sr_5(PO_4)_3F$ host

I.M. Nagpure[a,b,*], S.J. Dhoble[b], Manoj Mohapatra[c], Vinay Kumar[a], Shreyas S. Pitale[a], O.M. Ntwaeaborwa[a], S.V. Godbole[c], H.C. Swart[a,**]

[a] Department of Physics, University of the Free State, P.O. Box 339, Bloemfontein 9300, South Africa
[b] Department of Physics, RTM Nagpur University, Nagpur 440 033, India
[c] Radiochemistry Division, Bhabha Atomic Research Centre, Mumbai 400085, India

ARTICLE INFO

Article history:
Received 7 September 2010
Received in revised form
10 November 2010
Accepted 14 November 2010
Available online 19 November 2010

Keywords:
Phosphors
XRD
EDS
SEM
Photoluminescence
TRES

ABSTRACT

Europium (Eu^{3+}) activated strontium fluoropatite ($Sr_5(PO_4)_3F$) phosphor powders were prepared by a combustion method. The structure and luminescence properties of this potential red emitting phosphor are explored. In order to improve the luminescent properties the obtained powders were also annealed at 900 and 1200 °C. The X-ray diffraction (XRD) data indicated that the major crystalline phases from the as-prepared or annealed powder samples were identical to the hexagonal apatite structure of $Sr_5(PO_4)_3F$. The Eu^{3+} occupied two different sites (C_s (S1) and C_3 (S2)) of Sr in the $Sr_5(PO_4)_3F$ host, giving rise to two emission sites, as inferred from the time resolved luminescence spectroscopy (TRES) data. The photoluminescence (PL) intensity of Eu^{3+} from the as prepared sample was found to be more intense than the annealed samples. In addition from the PL data it was evident that a reduction of the Eu^{3+} to Eu^{2+} occurred.

1. Introduction

Spectroscopic properties of trivalent rare-earth (RE) ions such as Pr^{3+}, Nd^{3+}, Ho^{3+}, Er^{3+} and Tm^{3+} incorporated crystals of strontium fluorapatite (SFAP) or $Sr_5(PO_4)_3F$ have been reported [1–3]. These studies were motivated by the potential use of SFAP either as a laser host material, or as a saturable switch absorber [4]. In this study, the optical properties of Eu^{3+} activated $Sr_5(PO_4)_3F$ as a prominent red emitting phosphor were investigated for applications such as fluorescence or electroluminescence lamps [5], electronic information display devices and light emitting diodes (LEDs) [6]. The interesting and useful properties observed in apatites depend on the occurrence of minor substitution that lead to minor alterations in the ideal apatite structure. The ideal apatite SFAP crystallizes into the hexagonal system with a uni-axial lattice that belongs to the crystallographic group $P_{63/m}$ [7]. There are two non-equivalent crystallographic sites for the Sr, namely Sr^1 (Sr in a column) at $z = 0$ and 3/4, and Sr^2 (Sr screw axis) at $z = l/4$ and 3/4. In each unit cell four Sr^1 atoms, located on the threefold axis, are coordinated by six oxygen atoms as nearest neighbors belonging to the PO_4 group [8]. The site S(1), occupied by Sr^1 atoms is at the 4f Wyckoff position (C_3 symmetry). The other six Sr^2 atoms in the unit cell are coordinated by six oxygen atoms from the PO_4 tetrahedra and by one F^- ion located on the sixfold axis. The site S(2), occupied by Sr^2 is at the 6 h Wyckoff position (C_s symmetry). On the other hand, the F^- ions, occupy the 2a Wyckoff position (0, 0, 0.25) in the planes of the triangles formed by Sr^2. Thus, the apatite's structure can be represented as $[Sr^1]_4[Sr^2]_6(PO_4)_6F_2$ [9]. This structure can accommodate a variety of substitutions like rare earths, transition metals and alkaline earths forming an interesting set of compounds.

There are few reports on Eu^{3+} luminescence from fluroapatite [10,11] and oxyapatite [12] where, usually, an intense $^5D_0$–$^7F_0$ emission has been reported indicating a strong linear crystal-field component of the Eu^{3+} ion. Looking in terms of site occupancy and the charge compensation model, the $^5D_0$–$^7F_0$ emission is present when the Eu^{3+} ion occupies both the sites, i.e. Sr^1 and Sr^2, but is usually stronger with its Sr^2 site occupancy. This situation is further favored when the charge compensation occurs by an oxygen ion on the fluorine site. The intense $^5D_0$–$^7F_0$ transition gives rise to yellow-red emission [13,14]. Although, this transition allows significant insights in the local structural site symmetries, yet, it has a limited spectroscopic advantage in terms of a prominent

* Corresponding author at: Department of Physics, University of The Free State, P.O. Box 339, Campuslane South, Nelson Mandela Extention, Bloemfontein 9300, South Africa. Tel.: +27 51 401 2926; fax: +27 401 3507.
** Corresponding author.
E-mail addresses: indrajitnagpure@yahoo.co.in (I.M. Nagpure), swarthc@ufs.ac.za (H.C. Swart).

0925-8388/$ – see front matter © 2010 Elsevier B.V. All rights reserved.
doi:10.1016/j.jallcom.2010.11.086

red emitting phosphor. As an interest to the phosphor industry, the suppression of the $^5D_0$–$^7F_0$ yellow emission line is required, whereby subtle adjustments to the crystal field and distortion of local site symmetries play a vital role.

In the present case, investigations were done on prominent red emitting Eu^{3+} doped SFAP prepared by the combustion method to study the relation between structural and optical properties and their dependence on temperature and chemical composition. In particular, the occupation mode of Eu^{3+} ions on the 4f and 6h positions and that of the F^- ions on the 2a lattice positions in the apatite structure of the $Sr_5(PO_4)_3F$ phosphors were of interest. Moreover, interest in this phosphate based system comes from its potential use as a prominent red light emitting phosphor. A study on the chemical stability is also very important to test the application value of this material. A manuscript dealing with the stability issue will follow soon.

2. Experimental

$Sr_5(PO_4)_3F:Eu^{3+}$ phosphors were prepared via the combustion method using urea as a fuel. All the chemicals used in the phosphor preparation were of 99.99% purity. The starting materials were strontium nitrate ($Sr(NO_3)_2{\cdot}4H_2O$), diammonium hydrogen phosphate ($NH_4H_2(PO_4)$), ammonium fluoride (NH_4F) and Eu nitrate $Eu(NO_3)_3{\cdot}6H_2O$. All the reagents in required amounts were dissolved in appropriate solvents and mixed together to obtain a homogeneous solution. Urea (NH_2CONH_2) was dissolved in water. The ratio of the metal nitrates (oxidizers) and urea (fuel) was calculated using the total oxidizing and reducing valencies of the components, which served as the numerical coefficients to get an equivalent ratio of unity. To avoid an incomplete combustion reaction excess quantity of urea was added in the reaction mixture and an excess heat was liberated during the combustion process [15]. Urea solution was added to the metal nitrate solutions with vigorous stirring. The chemical reaction taking place in the combustion process can roughly be described as follows:

$$3OSr(NO_3)_2 + 18NH_4H_2(PO_4) + 6NH_4F + 29NH_2CONH_{2(excess)} + Eu(NO_3)_3 \cdot 6H_2O_{(m\%)} \rightarrow 6Sr_5(PO_4)_3F : Eu_{m\%} + 80N_2 + 29CO_2 + 151H_2O$$

After stirring for about 30 min, a semi-solid mass was obtained. This mass was transferred to a muffle furnace preheated at 500–600 °C and after 5 min a porous product was obtained which was designated as the as-prepared sample. $Sr_5(PO_4)_3:Eu^{3+}$ samples were prepared with different concentrations (0.1, 0.5, 1 and 2 mol%) of Eu^{3+} ions. The samples were annealed at 900 or 1200 °C to evaluate the effect of temperature on the structure and luminescence intensity.

The as-prepared (unannealed) and annealed powders were characterized by X-ray powder diffraction (XRD) in order to determine the phase purity and crystallinity. XRD analysis was carried out using a PAN-analytical diffractometer with Cu-K_λ (λ = 1.5418 Å) X-rays at a scanning step of 0.01°; scanning time at each step-20 s, in the 2θ range from 10° to 60°. The morphology and chemical composition analyses were carried out using a Shimadzu's SSX-550 scanning electron microscope (SEM) and energy dispersive X-ray (EDS) spectrometer, respectively. The photoluminescence (PL) and lifetime decay and time resolved data of the phosphors were recorded using a CD-920 unit from Edinburgh Analytical Instruments, UK.

3. Results and discussion

3.1. Structural, compositional and morphostructural characterizations

XRD patterns of the as-prepared, 900 and 1200 °C annealed powder samples of the $Sr_5(PO_4)_3F:Eu_{1\ mol\%}$ were obtained as shown in Fig. 1. The small quantity of the doped ions in the crystal did not change the crystal structure. Since Eu^{3+} has a smaller ionic radius of 0.947 Å compared to that of the Sr^{2+} (1.12 Å) ions, it can be easily incorporated into the Sr^{2+} sites. The XRD patterns showed characteristic reflections of the hexagonal apatite structure of $Sr_5(PO_4)_3F$ with $z = 2$ [9]. The patterns were compared with those of the standard JCPDs data file number No. 017-0609. An extra peak is observed in the XRD pattern of the $Sr_5(PO_4)_3F:Eu_{1\ mol\%}$ at 29.3° 2θ (labeled with a star). The experimental diffraction pattern was checked for the presence of impurity phases such as $Sr_2P_2O_7$ (JCPDs data file no 75-1490 as suggested by Toda [16] in $Sr_6BP_5O_{20}:Eu^{2+}$), $EuPO_4$ (JCPDs data file no. 18-0506) and $Eu_2O_3/Eu(NO_3)_3$ (JCPDs data file no. 31-0508). The extra impurity peak matches with the strongest diffraction line of the Eu_2O_3 phase [17]. The XRD patterns did not show any super lattice peaks and the full width at the half maxima (FWHM) varied only in a small range. The X-ray crystallography data of the $Sr_5(PO_4)_3F$ lattice is listed in Table 1. The experimental values of the *d*-spacings match reasonably well with the theoretical values as shown in Table 2. It seems that the FWHM of the as prepared sample is much broader than the annealed samples indicating that there was a relative increase in particle sizes due to the annealing process and the crystallinity of the samples

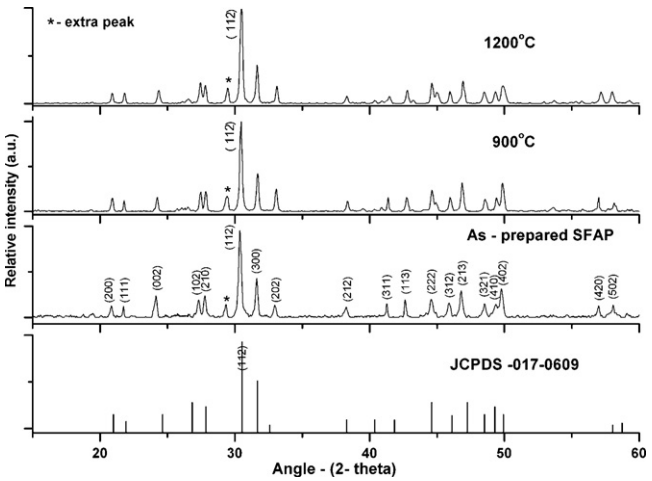

Fig. 1. XRD patterns of as prepared, 900 °C and 1200 °C heated $Sr_5(PO_4)_3F$ (SFAP) host.

Table 1
Crystallographic data for $Sr_5(PO_4)_3F$ (SFAP) lattice.

Phase	$Sr_5(PO_4)_3F$
Empirical formula	$Sr_5P_3O_{12}F$
Structure	Hexagonal (apatite)
Space group	$P_{63/m}$; $z = 2$
Formula weight	742.008 g/mol
Density	4.17 g/cm^3
Lattice parameter	
a (Å)	8.7350
b (Å)	9.29477
c (Å)	22.7789

$\alpha = \beta = 90° = \gamma = 120°$.

Table 2
h k l planes and *d*-spacing of $Sr_5(PO_4)_3F$ (SFAP) lattice.

h k l	*d*-Spacing (Å)			
	Theoretical	As-prepared	900 °C	1200 °C
2 0 0	4.230	4.228	4.233	4.231
1 1 1	4.050	4.049	4.055	4.051
0 0 2	3.610	3.605	3.609	3.608
1 0 2	3.320	3.322	3.319	3.323
2 1 0	3.200	3.203	3.201	3.202
1 1 2	2.901	2.905	2.904	2.903
3 0 0	2.822	2.820	2.824	2.827
2 0 2	2.745	2.743	2.745	2.746
2 1 2	2.404	2.406	2.403	2.401
3 1 1	2.232	2.231	2.233	2.230
1 1 3	2.157	2.155	2.157	2.156
2 2 2	2.023	2.021	2.023	2.024
3 1 2	1.967	1.964	1.968	1.963
2 1 3	1.922	1.924	1.223	1.927
3 2 1	1.875	1.877	1.879	1.872
4 1 0	1.847	1.846	1.843	1.849
4 0 2	1.825	1.827	1.828	1.822
4 2 0	1.600	1.601	1.603	1.604
4 0 3	1.588	1.585	1.587	1.589
5 0 2	1.533	1.534	1.536	1.533

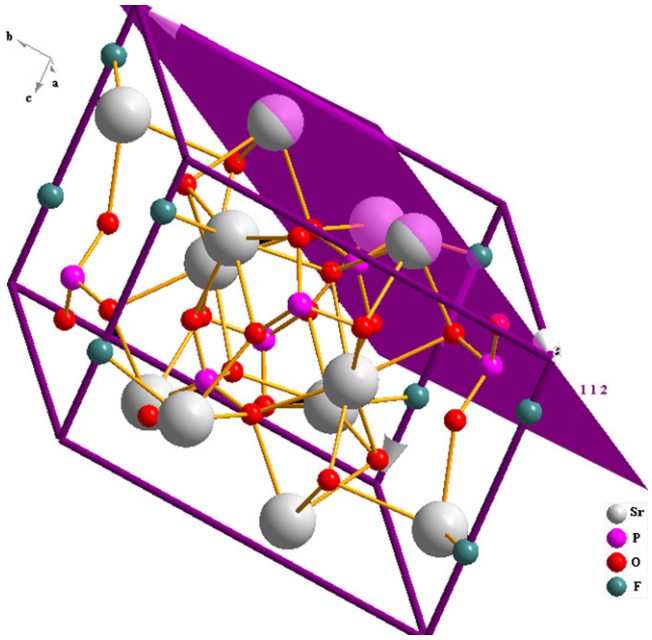

Fig. 2. Crystal structure of $Sr_5(PO_4)_3F$ (SFAP) host, strongest reflection coming from the plane (1 1 2) as indicated.

were improved during the annealing process.

A schematic of the ideal hexagonal apatite crystallite structure of $Sr_5(PO_4)_3F$ with the strongest reflection plane at (1 1 2) is shown in Fig. 2. The bond length between the divalent host metal ion (Sr^{2+}) and fluoride (F^-) in $Sr_5(PO_4)_3F$ is smaller than the sum of the ionic radii between the individual host metal and the F ion in the case of coordination number 7 [18]. Along the *c* axis, F1 anions occupy the 2a position in (I) and are coordinated by three equidistant Sr^2 atoms. In the apatite family the fluoroapatite has the highest symmetry with the space group corresponding to $P_{63/m}$ which can be attributed to the occurrence of fluoride ions in the planes of triangles constituted by alkaline earths [7]. Polarization of the Sr^{2+} divalent metal ions in the triangles by the small F^- ions could play the role in reducing the effective radius in the direction towards the F^- ion showing more effective photoluminescent properties. The number and position of the halide ions in the first coordination sphere of Sr ions depend on the fluoride content in the mixed crystals and at constant fluoride content, different Sr ions do not have the same surroundings of halide ions in their first coordination sphere in the range of $0 < x < 1$ [9]. The ionic radii of Eu ions are 94.7 pm for the coordination numbers 7, 8, or 9 [18]. Therefore, Eu^{3+} ions should occupy statistically both cation positions in the unit cell. From XRD measurements, it could not be decided whether Eu^{3+} ions prefer one of the two positions.

Major chemical elements, namely Sr, P, O, F and small amount of Eu were detected from the EDS data as shown in Fig. 3. Atomic percentages are consistent with expected results except for the O. From the weight and atomic percentage ratios the oxygen concentration is slightly higher than the expected value. This excess of oxygen in the crystal may be due to the trapping of gases in the porous structure during the combustion reaction. SEM micrographs of the as prepared and annealed SAFP samples are shown in Fig. 4(a)–(c). The effects of annealing on the morphology of SAPF are clearly observed. The as prepared $Sr_5(PO_4)_3F$ samples consisted of spherical particles which transformed to microporous coagulated fluffy particles after annealing.

3.2. PL investigation

3.2.1. Observations in the as-prepared sample

Fig. 5 shows the PL emission and excitation (inset) spectra of the as prepared SFAP samples with different concentrations of Eu^{3+}. The prominent excitation band at 243 nm may be due to the Eu^{3+}–O^{2-} charge transfer (CT) and the other smaller peaks as can be seen in the inset of Fig. 5 at 238, 263, 283 and 309 nm can be assigned to the 4f–4f transitions [19] of Eu^{3+}. The PL emission spectrum (λ_{exc} = 243 nm) consists of the major peak at 616 nm that can be ascribed to the $^5D_0 \rightarrow {}^7F_2$ transition of Eu^{3+} and other peaks at 590, 653, 680 and 705 nm to the $^5D_0 \rightarrow {}^7F_1$, $^5D_0 \rightarrow {}^7F_3$ and $^5D_0 \rightarrow {}^7F_4$ transitions of Eu^{3+}, respectively. The abnormal feature of the Eu-apatite structure appears as a shoulder and is observed at 578.7 nm corresponding to the $^5D_0 \rightarrow {}^7F_0$ transition [10–14]. The

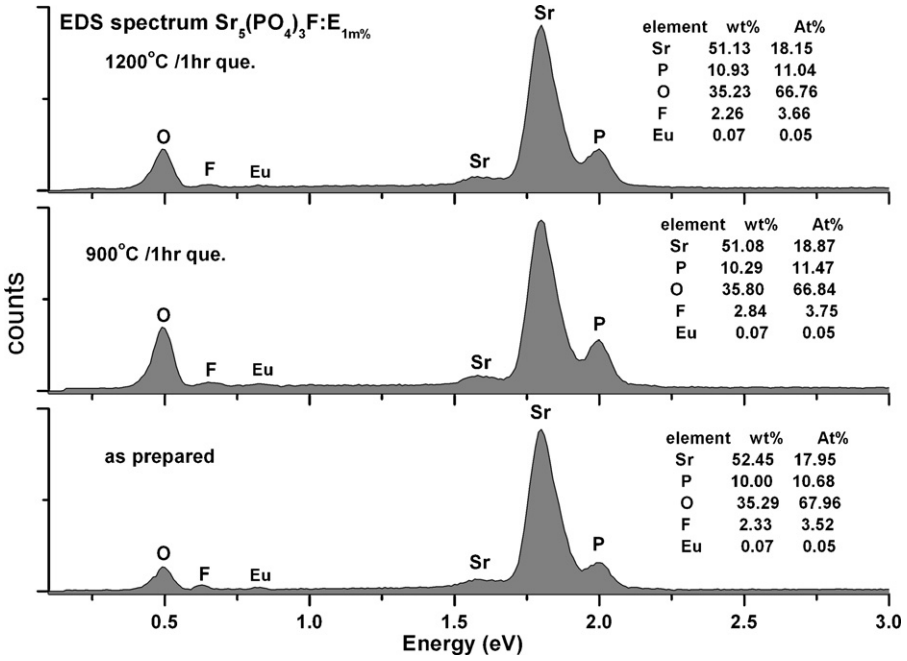

Fig. 3. SEM-EDS patterns of as prepared, 900 °C and 1200 °C heated $Sr_5(PO_4)_3F$ (SFAP) samples.

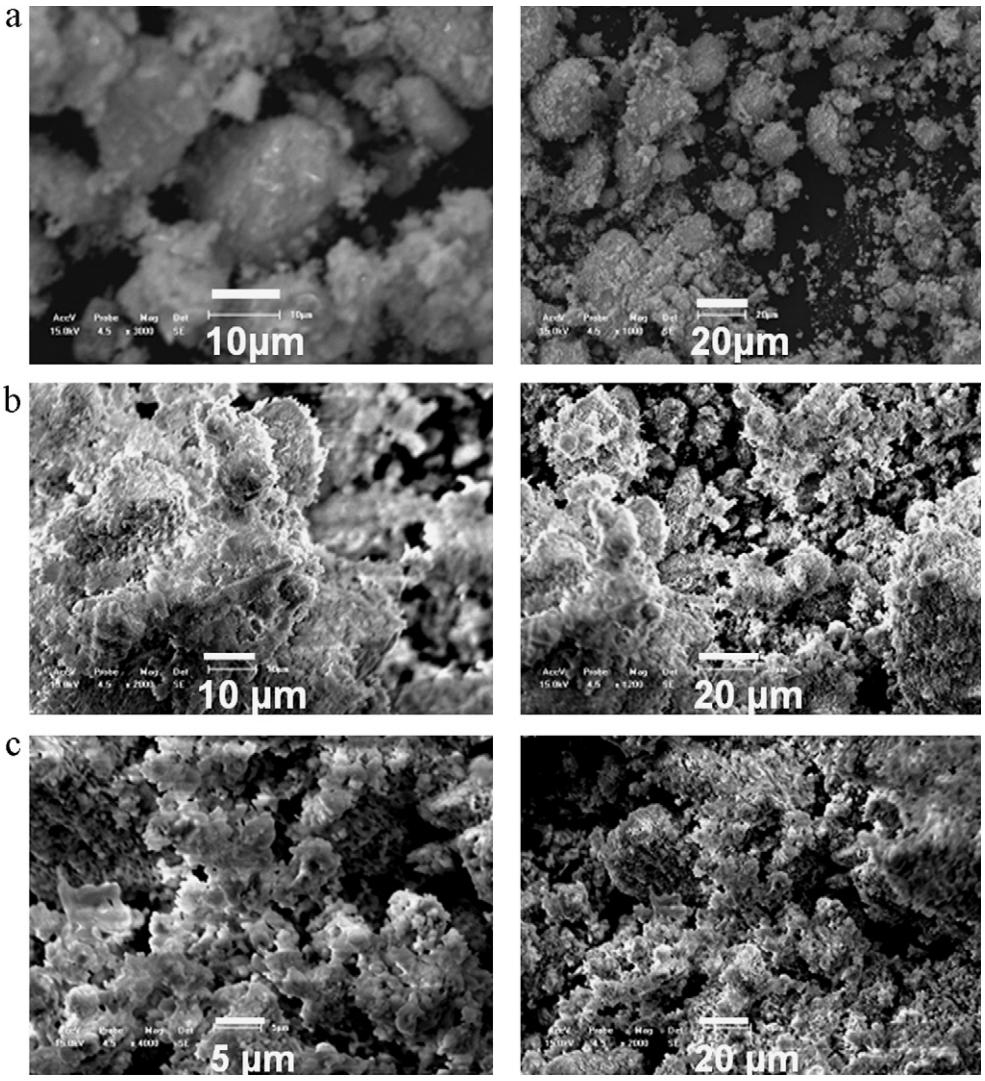

Fig. 4. (a) SEM images of $Sr_5(PO_4)_3F$ (SFAP) as prepared host. (b) SEM images of $Sr_5(PO_4)_3F$ (SFAP) host, at 900 °C for 1 h. (c) SEM images of $Sr_5(PO_4)_3F$ (SFAP) host, heated at 1200 °C for 1 h.

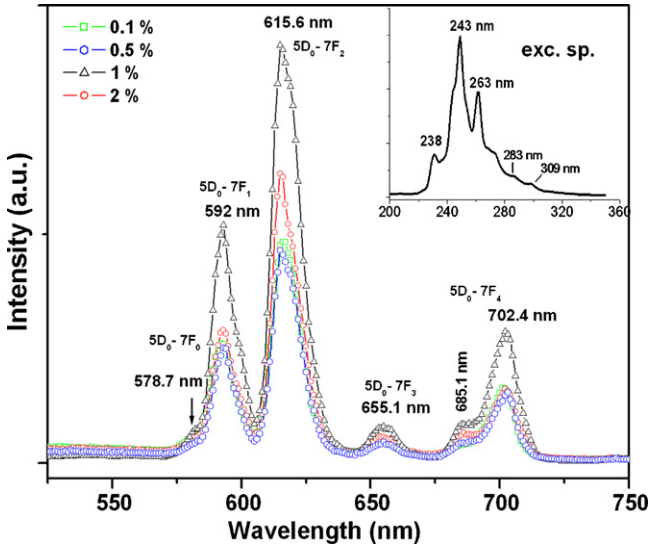

Fig. 5. PL emission intensity as the function of wavelength of as-prepared $Sr_5(PO_4)_3F:Eu_{0.1-2m\%}$, attributed to intraconfigurational $^5D_0$–^7F_J (J = 0–4) transitions monitored at λ_{ex} = 243 nm. (exc. sp. is shown in the inset).

$^5D_0 \rightarrow {}^7F_0$ transition is normally forbidden and will be present only when Eu^{3+} ion occupies sites with local symmetries of C_3 or C_s [12]. The $^5D_0 \rightarrow {}^7F_0$ line has been observed in the compounds with a strongly covalent Eu–O bond and this favors a higher intensity [14]. One can note that the intensity of the $^5D_0 \rightarrow {}^7F_0$ transition is weak in our case and it appears as a shoulder band at the same position as reported previously for an Eu-apatite structure [10–14]. The possibility of occurrence of pure red emission and suppression of the $^5D_0 \rightarrow {}^7F_0$ transition in the sample can be based on charge compensation and site symmetry distribution. We have performed a site-selective study of a particular level so that it is possible to see the distribution of Eu^{3+} in the S1 and S2 nonequivalent crystallographic sites in this material. The PL intensity increased with an increase in concentration from 0.5 to 1 mol% and it started to decrease at 2 mol% probably due to concentration quenching effects. From the emission spectrum, it seems that the $^5D_0 \rightarrow {}^7F_0$ transition is present as a shoulder in all the concentration and becomes prominent with higher Eu^{3+} concentrations. Note that further luminescence investigations were conducted only on the powder that gave the maximum PL intensity, i.e. the powder with the 1 mol% of Eu^{3+} doping. The PL spectrum from this powder is characterized by relatively major prominent emissions at 616 nm (red) and 590 nm (orange) and an abnormal non-degenerated emission at 578.7 nm as a shoulder. The red emission is associated

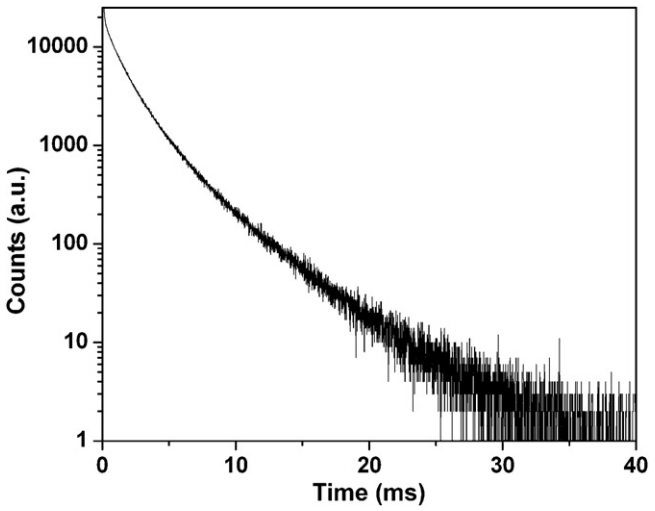

Fig. 6. Decay curve for the 1 mol% Eu doped as-prepared $Sr_5(PO_4)_3F$ (SFAP) sample.

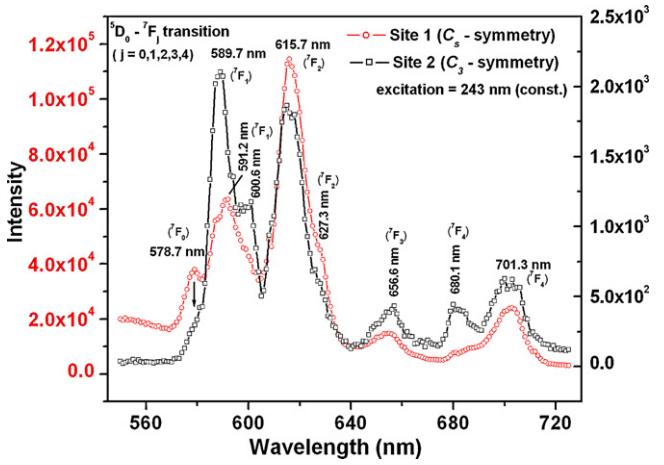

Fig. 7. Emission spectra of two sites of Sr^{2+} ion occupied by Eu^{3+} in the $Sr_5(PO_4)_3F$ (SFAP) host.

with the electric dipole transition with $\Delta J = \pm 2$, while the orange emission at 590 nm is a typical magnetic dipole transition. In the case of Eu^{3+}, the relative intensity of the 616 to the 590 nm peak strongly depends on the local site symmetry around the Eu^{3+} ions. A lower symmetry around Eu^{3+} ion would result in a higher I_{616}/I_{590} value, known as an asymmetric factor or asymmetric ratio [20]. In this case, the presence of a more intense red peak at 616 nm due to the $^5D_0 \rightarrow {}^7F_2$ transition, confirms that Eu^{3+} emission is parity forbidden and observed only when the lattice environment is distorted and contains non-inversion symmetry [21]. Being forced electric-dipole transition, this transition is hypersensitive to the environment.

As noted before Sr has two lattice sites, namely S1 and S2 that can be occupied by Eu^{3+} ions [22]. To get an idea about the exact nature of the dopant ion occupancy in these lattice sites, fluorescence decay time studies were conducted. Fig. 6 shows the luminescence decay curve for the 1 mol% of Eu from the as prepared sample with $\lambda_{ex} = 243$ nm and $\lambda_{em} = 616$ nm. The lifetime data could be fitted into a bi-exponential decay curve via the following equation:

$$I(t) = A + B_1 \exp\left(\frac{-t}{\tau_1}\right) + B_2 \exp\left(\frac{-t}{\tau_2}\right)$$

where A, B_1 and B_2 are scalar quantities, t is the time and $\tau_{1,2}$ are the decay time values. A best fit with probability $\chi^2 \approx 1.1$ was obtained for decay time values of $\tau_1 = 1.5$ and $\tau_2 = 3.9$ ms which are consistent with the lifetime values reported in the literature [23]. The presence of larger τ_2 values suggests that two components are responsible for the decay time. The faster component associated with the $^5D_0 \rightarrow {}^7F_2$ state of the Eu^{3+} ion is expected to be exponential having a decay constant around 1.5 ms in the SFAP host with 60% contribution to the overall decay process. When Eu ion resides on the S1 site of the Sr^{2+} ion and the 2nd component (3.9 ms) suggests the presence of an additional relaxation process (40% to the total contribution) affecting the relaxation rate of the higher excited states of the activator in this phosphor system. The slower component of S1 is associated with slow transfer of charge carrier before recombination on the luminescence center. It is likely to arise from a quasi stable luminescence center of the S2 sites with longer life time. The origin of two contributions can be confirmed from the time resolved spectroscopy. According to several literature studies [12,14,24,25], Eu^{3+} substitutes Sr^{2+} ions and occupy mainly the S2 sites, with a relative abundance of 60% which makes $^5D_0 \rightarrow {}^7F_0$ transition more intense compared to other transition of Eu^{3+}. In our case observed $^5D_0 \rightarrow {}^7F_0$ emission band at 578.7 nm is related to S1 sites, with a relative abundance of 40%. It is very difficult to suggest the suppression of 578.7 nm peak due to above mentioned (60% and 40%) distribution of Eu in the S1 and S2 site. The charge compensation phenomenon also plays an important role in the suppression of the $^5D_0 \rightarrow {}^7F_0$ line. Modulation of I_{616}/I_{590} ratio as compared to the previous reports is a result of change in local site occupancies of the Eu^{3+} ion during the doping process rendering the phosphor with a better color purity and short decay time suitable for specific applications. The distributions of the Eu^{3+} ion in the prepared phosphors depend strongly on synthesis factors like the composition of the precursor mixtures, used fuel to oxidizer ratio and the ignition temperatures. The self-propagating exothermic nature of combustion reaction is very spontaneous and is benefited by small reaction time and faster reaction rate to form stable compounds. Owing to this nature, some thermodynamically permissible local lattice site rearrangement is possible which in turn affects the overall dopant distribution. This is in contrast to the previously reported $Sr_5(PO_4)_3F$:Eu and strontium apatite phosphors prepared via solid state and co-precipitation synthesis [10,11,13,14,24] where prominent presence of $^5D_0 \rightarrow {}^7F_0$ transitions was observed. This kind of synthesis usually precedes slowly allowing different lattice site stabilization and distributions. The optimum condition required for the complete suppression of $^5D_0 \rightarrow {}^7F_0$ transition while synthesizing phosphor under variable combustion process parameters is currently a subject of investigation.

Time resolved emission spectrometry provides a powerful tool for identifying multiple species present in a system. Time-resolved emission spectroscopy measurement of $Sr_5(PO_4)_3F$:$Eu_{1\ mol\%}$ luminescence is presented to obtain a better understanding of the emission characteristics of this phosphor. By virtue of triple resolution (excitation, emission and time resolution) systems having similar excitation and emission properties can also be differentiated. In the present case also, the occurrence of two life time values in the Eu doped SFAP sample suggested the presence of two types of lattice sites available for the Eu ions. Edinburg spectroflurophotometer with an ICCD detector was used to detect the fluorescence with a time delay set at 6 ms so as to obtain the contribution from long-lived component between the 1st (S1) and the 2nd (S2) lattice sites of the Sr^{2+} ion where Eu^{3+} can be accommodated. These two sites responsible for the two life time values were identified. Indeed with that time delay the (S1) lattice site which has a time constant of the order of 1.5 ms completely vanished and the 2nd (S2) lattice site should be detected. Fig. 7 shows the spectra of the Eu ions present in two different sites responsible for the respective decay times. It is worth noting that there is a drastic difference

between the sites as expected. The asymmetric ratio (I_{616}/I_{590}) values for site 1 is ~2.0 whereas for site 2 it is ~0.90 indicating that site 2 is more symmetric with respect to site 1. This observation is also evident from the fact that the $^5D_0 \rightarrow {}^7F_0$ transition (at 578.7 nm) is only observed in the case of site 1. The 0 to 0 transition is purely of electric dipole in nature, in a symmetric system, and it is difficult to be observed according to the Judd–Ofelt theory. While in an asymmetric system such as in site 1 it is expected to be observed. It is well known as indicated above that there are two types of Sr^{2+} sites in the crystal and probably the Eu ion is replacing the Sr in these two sites. From the correlation of the crystal structure data of SFAP and the luminescence investigations it was concluded that 60% of the trivalent Eu ions are occupying C_s symmetry and the other 40% ions are occupying a more symmetric C_3 symmetry and hence the overall emission spectrum is predominantly that of an asymmetric one. The site symmetry might have changed because of the charge-compensating species and the transition probability for these transitions of the Eu^{3+} occupying the S1 sites may be low. The geometry of the system should be closer to the centrosymmetric system in which case the electric dipole transition is expected to be forbidden [26]. This will, however, have a minimum effect due to the geometry of the S1 symmetric site (C_3) that remains intact. The high emission intensity from the S2 site may be due to an intense resonant transfer to the Eu^{3+}(S2) asymmetric site (C_s) [27]. Furthermore it appears that the relative abundance of the S1 sites should be low compared with that of the Eu^{3+}(S2) site. This seems to be possible because the excitation spectrum used to monitor these lines leads to a similar pattern that is comparable to that of the former, except that there is a change in the intensity ratio due to the distorted nature of the site [27]. The preference of Eu^{3+} for the S2 site agrees well with the model explained by Blasse [28] based on the electrostatic potential. It is therefore reasonable to conclude that Eu^{3+} in the SFAP system predominantly occupies the S2 sites and the intense resonant transfer from Eu^{3+}(S1) to Eu^{3+}(S2) makes the emission from S1 sites very weak.

When trivalent RE ions substituted divalent ions, charge compensation is required. The substitution gives rise to a distortion of the site symmetry allowing a stronger interaction of the $^5D_0$ and $^7F_0$ states with the charge transfer band of Eu^{3+} [29]. In this case $Sr_5(PO_4)_3F$ is a hexagonal apatite crystal structure with z = 2. The appearance of strong $^5D_0 \rightarrow {}^7F_0$ emission is related to the admixing of heavily odd-parity states into the $^5D_0$ and $^7F_0$ states through the crystal field potential leads to the breakdown of the closure approximation in the Judd–Ofelt theory. This is possible only in the case when the charge transfer band is taken as an admixing excited state and site symmetry is the lowest corresponding to the $^5D_0 \rightarrow {}^7F_0$ emission [29]. In our combustion synthesized Eu doped $Sr_5(PO_4)_3F$ sample, the extent of symmetry for the two sites S1 and S2 is different compared to the previously reported Eu doped fluroapatite [10,11]. The intense $^5D_0 \rightarrow {}^7F_0$ emission results from the charge neutrality between the Eu^{3+} in the Sr(II) site and the free O^{2-} ion. Therefore a strong covalent character of Eu^{3+}–O^{2-} bonding in the apatite structure is expected [13,14,30]. With majority of Eu^{3+} ions (60%) occupying a site S1 (4f) which lacks a pronounced linear crystal field term, the $^5D_0 \rightarrow {}^7F_0$ emission is very weak in our case even though the dopant is charge compensated by an oxygen ion on the fluorine site.

3.2.2. Observations in the annealed samples

Fig. 8 shows the PL emission spectra of the Eu ion doped SFAP samples as a function of the annealing temperature. It is clear from the spectra that with an increase in the annealing temperature, there is a reduction in the fluorescence intensity of the Eu signal along with the evolution of a weak signal at ~430–450 nm. The inset of Fig. 8 shows the enlarged portion of the 400–480 nm part of the spectra. This is typical behavior of Eu^{2+} originating from inter

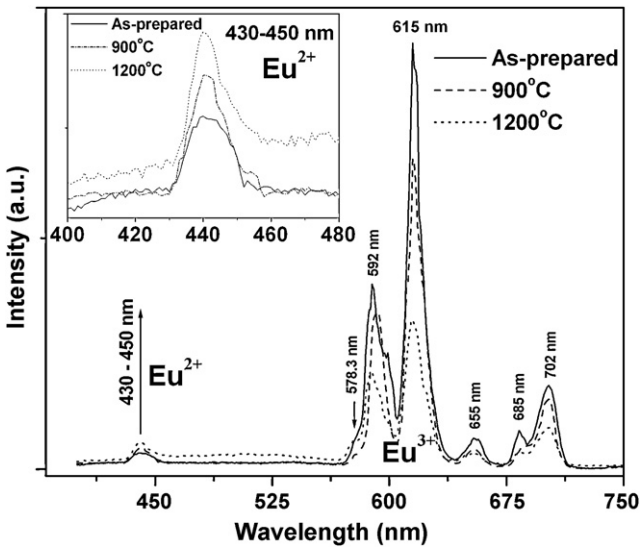

Fig. 8. Emission spectrum of the $Sr_5(PO_4)_3F:Eu_{1m\%}$ sample as function of annealing temperature.

electronic rearrangement ($4f^6$ 5d to $4f^7$ ground state) [28]. With the increase in annealing temperature, the PL due to the Eu^{3+} intensity decreased and the PL from the Eu^{2+} intensity increased suggesting a reduction of Eu^{3+} to Eu^{2+} in the system.

The inter electronic rearrangement taking place in the divalent Eu ion is both laporte and spin allowed (being an f–d transition) and is expected to be very fast (of the order of nanoseconds). In fact, the divalent Eu is reported to have decay time values in the range of a few hundreds of nanoseconds to a few microseconds [31]. The decay characteristics of the 440 nm peak (λ_{exc} = 243 nm) were investigated. The decay curve obtained was fitted with a single exponential equation. Fig. 9 shows the decay profile where a decay time of 500 ns was obtained as the best fit value for the Eu^{2+} fluorescence decay times. This observation further confirms the presence of Eu^{2+} in the system and is the best match with the life time of Eu^{2+} ion doped different phosphors reported by Särner et al. [32].

Table 3 gives the asymmetric intensity ratios of the spectra obtained for the annealed samples. It is evident from the table that as the annealing temperature is increased; there is an decrease in the I_{616} value with respect to I_{590} suggesting that, Eu^{3+} is more

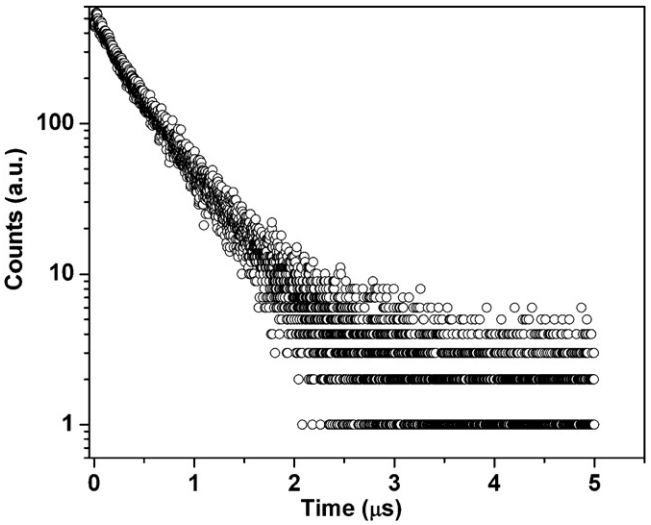

Fig. 9. Decay time curve for the Eu^{2+} ion in $Sr_5(PO_4)_3F$ as-prepared host.

Table 3
Asymmetric intensity ratio (I_{616}/I_{590}) $Sr_5(PO_4)_3F$:Eu (SFAP) sample as function of annealing temperature.

Sample	Asymmetric intensity ratio (I_{616}/I_{590})
As-prepared	2.31
900 annealed	1.97
1200 annealed	1.54

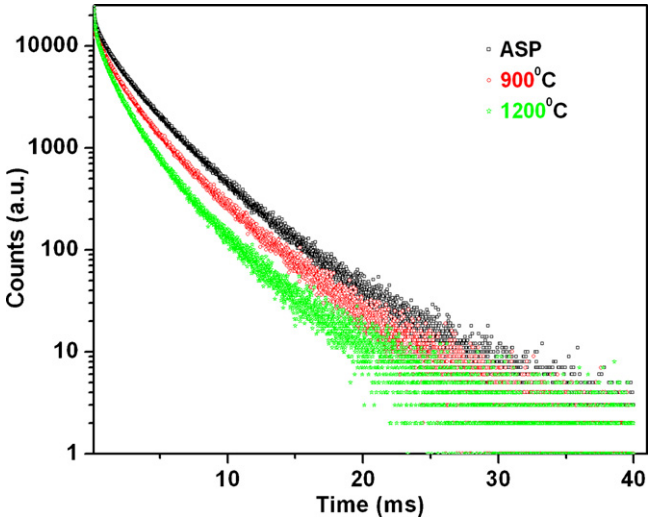

Fig. 10. Decay time curves for the $Sr_5(PO_4)_3F:Eu_{1m\%}$ in as-prepared and annealed samples.

preferentially going to the symmetric site (C_3) rather than to the asymmetric one (C_s) as mentioned from the time resolved emission spectrum. Which means that, Eu^{3+} ions present in the distorted environment gets preferentially reduced to the divalent ion as compared to the ions present in a symmetric state. The crystallites with two different lattice sites in the Sr^{2+} host contribute to the presence of defects on the surface and annealing directly affecting the lifetime values. Therefore, the defect produced via annealing in the system can be responsible for the overall lifetime of Eu^{3+} ion due to the contribution of the increasing non-radiative process. Since no external reagent was used, in the system which could lead to the reduction, it can be argued that the reduction of the lanthanide ion is brought about by a process which can best be described as defect mediated. Such type of defect center mediated reduction is well reported by several workers [33]. Since the Eu^{3+} ion in disordered environment, gets reduced preferentially, it can be said that, these type of ions are in the vicinity of the defect centers. And the 3+ ions in the symmetric environment are away from the defect centers so that they are not reduced. This argument is further supported by the decay time experiments performed on the annealed samples. Fig. 10 gives a comparison of the decay time graphs for the as prepared, 900 and 1200 annealed samples whose details are listed in Table 4.

Table 4 shows the two decay time values obtained for the as prepared as well as annealed samples. The figures within the bracket are the relative percentages of the individual components. It can be observed from the data that with an increase in the annealing temperature, the component with longer decay time is in fact reducing. The component with shorter decay time is increasing with no significant change in the decay time values. This also suggests that Eu^{3+} is getting converted into the divalent species preferentially from the site with longer decay time, i.e. with a distorted geometry (C_s). It is worth noting that by annealing at the higher temperatures, there was no change in the decay time values for the divalent ion indicating that, there is only one type of Eu^{2+} present in the system.

Table 4
Decay time values and relative percentage of $Sr_5(PO_4)_3F:Eu_{1m\%}$ in as-prepared and annealed samples.

Sample	τ_1 (ms)	τ_2 (ms)
As-prepared	1.54 (60%)	3.91 (40%)
900	1.39 (53%)	3.80 (47%)
1200	1.43 (48%)	3.85 (52%)

4. Conclusion

Eu doped strontium fluorapatite was synthesized via the combustion method using urea as the fuel element. It was characterized by XRD, EDS, SEM and PL techniques. The maximum PL intensity was observed from the sample with 1 mol% of Eu^{3+} co-doping. Eu^{3+} occupied two different sites in the $Sr_5(PO_4)_3F$ matrix, namely S1 and S2 with the relative ratios of 60 and 40%, respectively. The major fraction of the trivalent ion was present in a disordered geometry (C_s) whereas the other portion was present in a symmetric environment (C_3). The charge compensation and site distribution play an important role in the suppression of the $^5D_0 \rightarrow {}^7F_0$ yellow line and $^5D_0 \rightarrow {}^7F_2$ emission line appeared as a prominent red emission. After annealing at 900 and 1200 °C a reduction in the Eu^{3+} PL intensity with the increase in asymmetric ratio was observed. The formation of Eu^{2+} in the system upon annealing the sample was also observed. It can be concluded that the Eu^{3+} was reduced to Eu^{2+} preferably from a position which is near to the defect centers.

Acknowledgements

The authors are thankful to Prof. V.K. Manchanda, Head; Radiochemistry Division, BARC for his interest and encouragement to carry out this work. One of the authors, SJD is thankful to BRNS (No. 2005/37/19/BRNS/1745), Department of Atomic Energy, Government of India, for the financial assistance. The financial supports of the University of the Free State (UFS) and the National Research Foundation and Centre for Microscopy at UFS for SEM/EDS are gratefully acknowledged. Authors are thankful to Dr. M.K. Bhide, Dr. K.N. Shinde for their kind help during the research work.

References

[1] P. Dorenbos, J. Phys. Condens. Matter 15: (2003) 2645.
[2] A.A. Kaminskii, Laser Photon. Rev. 1 (2007) 93.
[3] A.O. Wright, M.D. Seltzer, J.B. Gruber, B.H.T. Chai, J. Appl. Phys. 78 (1995) 2456.
[4] P. Li, Q.P. Wang, X.Y. Zhang, S.Z. Zhao, D. Gao, X.M. Liu, L.K. Sun, S.J. Zhang, B.B. Huang, B.F. Lin, F.W. Zhang, Chin. J. Lasers B 9 (2) (2000) 107.
[5] S. Ekambaram, M. Maaza, J. Alloy. Compd. 395: (2005) 132.
[6] K.U. Kim, S.H. Choi, H.-K. Jung, S. Nahm, Developments in Strategic Materials, 28, Wiley Interscience, 2009, p. 278.
[7] D. Noĕtzold, H. Wulff, Phys. Stat. Sol. (b) 207 (1998) 271.
[8] D. Noĕtzold, H. Wulff, G. Herzog, Phys. Stat. Sol. (b) 191: (1995) 21.
[9] A.N. Akhavan-Niaki, Ann. Chim. (France) (1961) 51.
[10] A. Zounani, D. Zambon, J.C. Cousseins, J. Alloys Compd. 188 (1992) 82.
[11] A. Zounani, D. Zambon, J.C. Cousseins, J. Alloys Compd. 207 (1994) 94.
[12] R. Ternane, G. Panczer, Cohen-Adad MTh, C. Goutaudier, G. Boulon, N.K. Ariguib, M.T. Ayedi, Opt. Mater. 16 (1-2) (2001) 291.
[13] B. Piriou, D. Fahmi, J. Dexpert-Ghys, A. Taitai, J.L. Lacout, J. Lumin. 39 (1987) 97.
[14] N. Lakshminarasimhan, U.V. Varadaraju, J. Solid State Chem. 177 (2004) 3536.
[15] S. Gallini, J.R. Jurado, M.T. Colomer, Chem. Mater. 17 (2005) 4154.
[16] K. Toda, J. Alloys Compd. 408 (2006) 665.
[17] J. Poth, R. Haberkorn, H.P. Beck, J. Eur. Ceram. Soc. 20 (2000) 715.
[18] R.D. Shannon, Acta Cryst. A 32 (1976) 751.
[19] B.N. Mahalley, S.J. Dhoble, R.B. Pode, G. Alexander, Appl. Phys. A 70 (2000) 39.
[20] P. Dorenbos, L. Pierron, L. Dinca, C.W.E. van Eijk, A. Kahn-Harari, B. Viana, J. Phys. Condens. Matter 15 (2003) 511.
[21] V. Natarajan, M.K. Bhide, A.R. Dhobale, S.V. Godbole, T.K. Seshagiri, A.G. Page, C.-H. Lu, Mater. Res. Bull. 39 (2004) 2065.
[22] G. Blasse, J. Solid State Chem. 4 (1972) 52.

[23] C. Zhang, J. Yang, C. Lin, C. Li, J. Lin, J. Solid State Chem. 182 (7) (2009) 1673.
[24] R. Ternane, M. Trabelsi-Ayedi, N. Kbir-Ariguib, B. Piriou, J. Lumin. 81 (1999) 165.
[25] Ouenzerfi ElR, N. Kbir-Ariguib, M. Trabelsi-Ayedi, B. Piriou, J. Lumin. 85 (1999) 71.
[26] G. Blasse, J. Solid State Chem. 14 (1975) 181.
[27] R. Jagannathan, M. Kottaisamy, J. Phys. Condens. Matter 7 (1995) 8453.
[28] G. Blasse, Lumin. Inorg. Solids 475 (1978) 215.
[29] L.S. Geigerova, O.F. Dudnik, V.F. Zolin, V.A. Kudryashova, in: F. Williams (Ed.), Luminescence of Crystals, Molecules and Solutions, Academic, New York, 1973, p. 514.
[30] T. Hoshina, S. Imanaga, S. Yokono, J. Lumin. 15 (1977) 455.
[31] W.M. Yen, S. Shionoya, H. Yamamoto, Phosphor Handbook, 2nd ed., CRC Press, New York, 2007.
[32] G. Särner, M. Richter, M. Aldén, Meas. Sci. Technol. 19 (2008) 125304.
[33] J.L. Ferrari, A.M. Pires, M.R. Davolos, Mater. Chem. Phys. 113 (2009) 587.